







RESEARCH ARTICLE

Sensitivity of Advanced Magnetic Resonance Imaging to Progression over Six Months in Early Spinocerebellar Ataxia

Thiago J.R. Rezende, PhD,¹  Emilien Petit, PhD,²  Young Woo Park, PhD,³ Sophie Tezenas du Montcel, MD, PhD,² James M. Joers, PhD,³ Jonathan M. DuBois, PhD,⁴ H. Moore Arnold, PhD,⁴ Michal Povazan, PhD,⁵ Guita Banan, PhD,⁶ Romain Valabregue, PhD,² Philipp Ehse, PhD,⁷ Jennifer Faber, MD, PhD,^{7,8} Pierrick Coupé, PhD,⁹ Chiadi U. Onyike, MBBS, MD,⁵ Peter B. Barker, PhD,⁵ Jeremy D. Schmahmann, MD,¹⁰  Eva-Maria Ratai, PhD,¹¹ Sub H. Subramony, MD,⁶ Thomas H. Mareci, PhD,⁶ Khalaf O. Bushara, MD,³ Henry Paulson, MD, PhD,¹² Thomas Klockgether, MD,^{7,8}  Alexandra Durr, MD, PhD,² Tetsuo Ashizawa, MD,¹³  Christophe Lenglet, PhD,³ Gülin Öz, PhD,^{3*}  READISCA Consortium

¹Department of Neurology, School of Medical Sciences, University of Campinas, Campinas, Brazil

²Sorbonne Université, Paris Brain Institute, Inserm, INRIA, CNRS, APHP, Paris, France

³Department of Radiology, Center for Magnetic Resonance Research, University of Minnesota, Minneapolis, Minnesota, USA

⁴Biogen, Cambridge, Massachusetts, USA

⁵Department of Radiology, Johns Hopkins University, School of Medicine, Baltimore, Maryland, USA

⁶Norman Fixel Center for Neurological Disorders, College of Medicine, University of Florida, Gainesville, Florida, USA

⁷German Center for Neurodegenerative Diseases (DZNE), Bonn, Germany

⁸Department of Neurology, University Hospital Bonn, Bonn, Germany

⁹Laboratoire Bordelais de Recherche en Informatique, Université de Bordeaux, Talence, France

¹⁰Laboratory for Neuroanatomy and Cerebellar Neurobiology, Department of Neurology, Ataxia Center, Massachusetts General Hospital and Harvard Medical School, Boston, Massachusetts, USA

¹¹A. A. Martinos Center for Biomedical Imaging, Massachusetts General Hospital, Department of Radiology, Harvard Medical School, Boston, Massachusetts, USA

¹²Department of Neurology, University of Michigan, Ann Arbor, Michigan, USA

¹³Department of Neurology, The Houston Methodist Research Institute, Houston, Texas, USA

ABSTRACT: Background: Clinical trials for upcoming disease-modifying therapies of spinocerebellar ataxias (SCA), a group of rare movement disorders, lack endpoints sensitive to early disease progression, when therapeutics will be most effective. In addition, regulatory agencies emphasize the importance of biological outcomes.

Objectives: READISCA, a transatlantic clinical trial readiness consortium, investigated whether advanced

multimodal magnetic resonance imaging (MRI) detects pathology progression over 6 months in preataxic and early ataxic carriers of SCA mutations.

Methods: A total of 44 participants (10 SCA1, 25 SCA3, and 9 controls) prospectively underwent 3-T MR scanning at baseline and a median [interquartile range] follow-up of 6.2 [5.9–6.7] months; 44% of SCA participants were preataxic. Blinded analyses of annual changes in structural, diffusion MRI, MR spectroscopy, and the

This is an open access article under the terms of the [Creative Commons Attribution-NonCommercial-NoDerivs](#) License, which permits use and distribution in any medium, provided the original work is properly cited, the use is non-commercial and no modifications or adaptations are made.

*Correspondence to: Dr. Gülin Öz, Department of Radiology, Center for Magnetic Resonance Research, University of Minnesota, 2021 Sixth Street Southeast, Minneapolis, MN 55455, USA; E-mail: gulin@cmrr.umn.edu

Relevant conflicts of interest/financial disclosures: This work was supported by the National Institute of Neurological Disorders and Stroke (NINDS) grant U01 NS104326 and Biogen. The Center for Magnetic Resonance Research is supported by the National Institute of Biomedical Imaging and Bioengineering (NIBIB) grant P41 EB027061 and the National Institute of Neurological Disorders and Stroke (Institutional Center Cores for Advanced Neuroimaging award) grant P30 NS076408 and Office of The Director, National Institutes of Health grant S10OD017974. Research reported in this publication was also

supported by an Academic Investment Research Program (AIRP) award at the University of Minnesota and the National Center for Advancing Translational Sciences of the National Institutes of Health Award Number UL1TR000114. A portion of this work was performed in the McKnight Brain Institute of the University of Florida at the National High Magnetic Field Laboratory's Advanced Magnetic Resonance Imaging and Spectroscopy (AMRIS) Facility, which is supported by the National Science Foundation Cooperative Agreement DMR-1644779 and the State of Florida and was supported in part by an NIH award, S10 OD021726, for High End Instrumentation. The content is solely the responsibility of the authors and does not necessarily represent the official views of the National Institutes of Health.

Received: 10 April 2024; **Revised:** 11 June 2024; **Accepted:** 2 July 2024

Published online 26 July 2024 in Wiley Online Library (wileyonlinelibrary.com). DOI: 10.1002/mds.29934

Scale for Assessment and Rating of Ataxia (SARA) were compared between groups using nonparametric testing. Sample sizes were estimated for 6-month interventional trials with 50% to 100% treatment effect size, leveraging existing large cohort data (186 SCA1, 272 SCA3) for the SARA estimate.

Results: Rate of change in microstructural integrity (decrease in fractional anisotropy, increase in diffusivities) in the middle cerebellar peduncle, corona radiata, and superior longitudinal fasciculus significantly differed in SCAs from controls ($P < 0.005$), with high effect sizes (Cohen's $d = 1-2$) and moderate-to-high responsiveness ($|\text{standardized response mean}| = 0.6-0.9$) in SCAs.

SARA scores did not change, and their rate of change did not differ between groups.

Conclusions: Diffusion MRI is sensitive to disease progression at very early-stage SCA1 and SCA3 and may provide a >5-fold reduction in sample sizes relative to SARA as endpoint for 6-month-long trials. © 2024 The Author(s). *Movement Disorders* published by Wiley Periodicals LLC on behalf of International Parkinson and Movement Disorder Society.

Key Words: READISCA; magnetic resonance imaging; longitudinal; biomarker; diffusion tensor imaging

Spinocerebellar ataxias (SCA) are rare neurodegenerative disorders that share cerebellar ataxia as their core clinical finding. SCA1 shows the fastest progression, whereas SCA3 is the most common worldwide.¹ Both are caused by CAG repeat expansions. There are no approved disease-modifying treatments for SCAs, but gene-silencing strategies are in the pipeline.² Such therapies are expected to be most effective in early disease prior to substantial neuronal loss.³ To enable clinical trials at early, including premanifest, stages, outcome measures sensitive to early pathological changes are needed. However, clinical rating scales, such as the Scale for Assessment and Rating of Ataxia (SARA),⁴ are not sensitive to change in the earliest stages and over short, trial-relevant periods.⁵ Therefore, trials designed with clinical outcomes require large cohorts and/or long follow-ups,² a major barrier for these rare and slowly progressive diseases.

Neuroimaging may help overcome these limitations because it enables a direct and objective assessment of pathology. Furthermore, imaging and fluid biomarkers are increasingly used as primary and secondary outcomes in therapeutic trials⁶⁻⁸ and even serve as the basis for the U.S. Food and Drug Administration approvals.^{6,8} READISCA is a multisite longitudinal clinical trial readiness study that enrolls early-stage SCA1 and SCA3 mutation carriers and gene-negative controls to validate clinical and imaging outcomes in the academic trial setting (<https://clinicaltrials.gov/ct2/show/NCT03487367>). The study utilizes an advanced magnetic resonance imaging (MRI) protocol to achieve high precision in MRI outcomes and minimize the necessary sample sizes for upcoming SCA trials. Baseline READISCA MRI data demonstrated morphometric, microstructural, and neurochemical alterations in preataxic and early SCA1 and SCA3.⁹ The sensitivity of these MR measures to disease progression over short follow-up durations is unknown. Prior longitudinal studies in SCAs assessed patients at later disease stages or longer follow-ups, from 12 to 60 months.¹⁰⁻¹⁴

Here, we report the first prospective structural, diffusion MRI (dMRI) and MR spectroscopy (MRS)

findings in a subset of the READISCA cohort scanned ~6 months after baseline to determine if MR measures are sensitive to change over a trial-relevant follow-up period (Appendix A).

Patients and Methods

Study Design, Participants, and Clinical Assessment

In this prospective longitudinal case-control study, 44 participants from the READISCA imaging cohort⁹ were scanned at baseline and after a median (interquartile range [IQR]) follow-up duration of 6.2 [5.9–6.7] months (Fig. 1; Table 1). The sample size was guided by feasibility and participant willingness to return as follow-up visits occurred from 2019 to 2021, mostly during the COVID-19 pandemic. Participants were enrolled at 12 sites and scanned at 6 sites (University of Minnesota, University of Florida, Johns Hopkins University [JHU], Massachusetts General Hospital, German Center for Neurodegenerative Diseases, and ICM Paris Brain Institute). The enrollment criteria were described previously⁹ and targeted participants with SARA <10 at baseline. SCA mutation carriers with SARA <3 were classified as preataxic.⁹ Control participants tested negative for SCA1 and SCA3 and were evaluated to rule out other neurological diseases. The SARA score⁴ was used to quantify ataxia severity at both visits. Ataxic participants reported their age at ataxia onset (Table 1). The time from ataxia onset at baseline was estimated using the CAG repeat length for all mutation carriers, as described previously.^{9,15,16}

The study was approved by the Institutional Review Board at each site, and informed consent was obtained. This study followed the Strengthening the Reporting of Observational Studies in Epidemiology (STROBE) reporting guidelines.

MRI Data Acquisition

The MRI protocol was described in the baseline READISCA publication.⁹ Briefly, data were acquired on

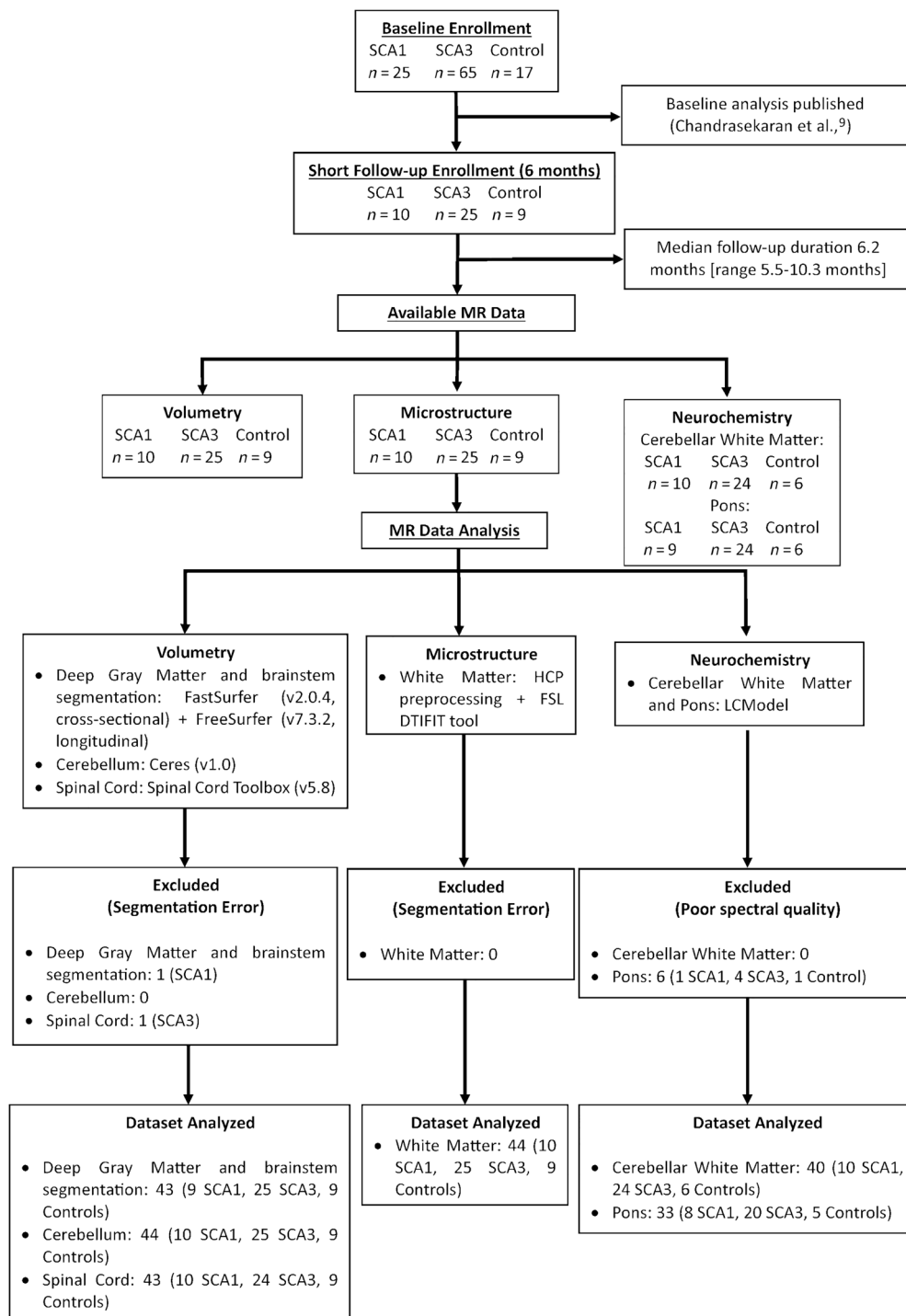


FIG. 1. Outline of enrollment, magnetic resonance (MR) analysis, and quality control.

3-T Siemens (Erlangen, Germany) scanners (5 Prisma, 1 Skyra) operating *Syngo MR E11* software and using body coil transmission and a 32-channel receive array. Structural and dMRI acquisitions were based on the Human Connectome Project (HCP) lifespan protocol¹⁷ and included the following sequences:

- 3D T1-weighted (T1w) MPRAGE: voxel size = 0.8 mm³ isotropic, repetition time (TR)/echo time (TE)/inversion

time 2400/2.2/1000 ms, flip angle = 8°, GRAPPA factor = 2;

- 3D T2-weighted (T2w) SPACE: voxel size = 0.8 mm³ isotropic, TR/TE 3200/563 ms, GRAPPA factor = 2;
- Multiband dMRI was acquired with opposing phase encoding in the anterior–posterior direction and *q*-space sampling split into two sets of 98 and two sets of 99 volumes, resulting in two sets of 197 volumes (including 13 *b* = 0 and 184 unique diffusion volumes). On

TABLE 1 Cohort characteristics at baseline, duration of follow-up, and SARA at baseline and follow-up

Group	Control (n = 9)	SCA1 (n = 10)	SCA3 (n = 25)	P*
Age (IQR) (y)	47 (34; 51)	47 (37; 54)	42 (37; 50)	0.68
Sex (female %)	3 (33%)	8 (80%)	15 (60%)	0.12
Follow-up duration (IQR), days	205 (179; 210)	208 (194; 248)	204 (191; 235)	0.54
Reported age at onset (IQR) (y) ^a	NA	40 (35.5; 46) n = 8	42.5 (30; 50) n = 12	0.84
Reported time from ataxia onset (IQR) (y)	NA	7.5 (3; 11.5) n = 8	4.5 (2.5; 11.5) n = 12	0.96
Estimated time from ataxia onset (IQR) (y) ^b	NA	5.4 (−0.6; 12) n = 9	4.3 (−0.74; 9.9)	0.71
CAG repeat length (IQR), long allele	NA	45 (43; 45) n = 9	71 (69; 73)	NA
SARA at baseline (IQR)	0 (0; 1)	7 (3.5; 8)	2 (1.5; 6.5)	0.001
SARA at follow-up (IQR)	0 (0; 0)	6.5 (5; 10)	3.5 (2; 6.5)	0.001
SARA change (IQR)	0 (0; 0)	0 (−1.5; 2)	0 (0; 1.5)	0.27
Number of preataxic participants (%)	NA	2 (20%)	13 (52%)	0.18

For categorical variables frequencies are provided using percentages, and for quantitative variables median and interquartile range (Q1; Q3) are provided; n is provided when values are reported by a subset of the cohort or are missing.

*P-values are the overall Kruskal–Wallis P-value for quantitative variables and the χ^2 P-value for categorical variables.

^aAge at onset reported only by individuals with ataxia symptoms.

^bEstimated time from ataxia onset is the difference between the ataxia onset age estimated for all participants using their CAG repeat length and the age at baseline.

Abbreviations: NA, not applicable; SARA, Scale for Assessment and Rating of Ataxia; IQR, interquartile range.

Prisma scanners: voxel size = 1.5 mm³ isotropic, TR/TE = 3230/89.2 ms, multiband acceleration = 4, b = 1500 and 3000 s/mm². On the Skyra scanner: voxel size = 1.7 mm³ isotropic, TR/TE = 3390/103.2 ms, multiband acceleration = 4, b = 1000 and 2000 s/mm².

MRS data were collected using an automated, harmonized semi-LASER protocol (TR/TE = 3000/30 ms, 80 transients)¹⁸ with integrated B₀ and B₁ calibration.¹⁹ The volumes of interest (VOI) were pons (16 × 16 × 16 mm³) and cerebellar white matter (CBWM, 17 × 17 × 17 mm³), which were automatically prescribed by AutoVOI.²⁰ One site had network issues preventing AutoVOI from functioning for most follow-up scans, which necessitated manual VOI placement. Unsuppressed water spectra were obtained as an internal quantification reference and for residual eddy current correction.

MR Quality Control and Preprocessing

The analytic workflow is shown in Figure 1. DICOM images were de-identified using *DicomBrowser* software,²¹ and T1w and T2w images were defaced using face masking²² on-site prior to uploading to a Flywheel (<https://flywheel.io/>) database running on a dedicated server at the University of Minnesota for centralized analysis. A Docker container was shared by the University of Minnesota team with the other imaging sites to automatically de-identify and upload the data.

MR data were analyzed blind to diagnosis. For quality control (QC) T1w and T2w data were scored 0 to 2 (pass = 0–0.25, check = 0.5–1, and fail = 1.25–2) considering

image sharpness, ringing, and contrast-to-noise ratio in subcortical, gray matter, and WM regions.^{9,23} The QC of the diffusion images was performed using an FSL EDDY QC tool,²⁴ which is an automated and quantitative diffusion MRI QC framework based on the FSL EDDY tool.²⁵ Briefly, imaging slices with signal loss caused by participant movement were detected and replaced by predictions made by a Gaussian process during eddy.²⁵ Intra-volume participant movement was corrected using slice-to-volume alignment.²⁶ Finally and following our baseline publication,⁹ single-shot sLASER spectra were corrected for frequency, phase, and eddy current errors before averaging using the *MRspa* software (<https://www.cmrr.umn.edu/downloads/mrspa/>).²⁷ Single-shot spectra with poor water suppression or phase fluctuation indicating participant movement were excluded from averaging. MRS data with VOIs misplaced manually or with a linewidth of the associated water reference broader than 15 Hz were excluded from the analysis. This linewidth exclusion criterion was higher than that used for the baseline READISCA paper (13 Hz) because the primary metabolites of interest, that is, metabolites that were hypothesized to be sensitive to longitudinal change (total N-acetylaspartate [tNAA], myo-inositol, and total creatine [tCr]), are reliably quantified using Cramér–Rao lower bounds (CRLBs) ≤5%, even in spectra with 13- to 15-Hz linewidths.

Volumetry

To compute subcortical volumes, T1w images were initially processed using the *FastSurfer* software (version 2.0.4),²⁸ a deep-learning-based solution that

replicates the *FreeSurfer*²⁹ pipeline analysis with improved speed and performance, especially for higher-resolution images.³⁰ Next, data were processed using the *FreeSurfer* longitudinal pipeline that utilizes a fixed intracranial volume (ICV) for each participant, which is obtained from the average of the baseline and follow-up ICVs, assuming no within-subject change (version 7.3.2).³¹⁻³³ To increase the reliability and statistical power in the longitudinal analysis, several processing steps are initialized from the within-subject template.³³

Brainstem volumes (including medulla oblongata, pons, midbrain, and superior cerebellar peduncle) were estimated using the longitudinal subregion segmentation module within *FreeSurfer* (version 7.3.2).^{34,35} The longitudinal pipeline is based on subject-specific atlases; that is, the segmentations of the different time points are jointly computed using Bayesian inference and treated equally to avoid processing bias.³⁴

For cerebellum volumetry, we used the CERES (*CERES-Ebellum Segmentation*, version 1.0) software. CERES is a multi-atlas-based segmentation tool dedicated to assess the cerebellum.³⁶ When compared to other tools, CERES exhibited superior repeatability/reproducibility and cerebellar fissure segmentation in images with cerebellar atrophy.^{37,38}

Finally, to evaluate the upper spinal cord, C1 and C2, we used a harmonized, open-source pipeline that was developed by the ENIGMA-Ataxia consortium (<http://enigma.ini.usc.edu/ongoing/enigma-ataxia/>),³⁹ based on the Spinal Cord Toolbox.⁴⁰ We opted to assess only C1 and C2 because the C3/C4 levels did not show adequate signal-to-noise ratio in some participants. Manual corrections were performed to correct spinal cord segmentation errors when necessary.

Region-of-Interest Analysis of Diffusion MRI

Following the same approach used in the cross-sectional analysis,⁹ we extracted the diffusion volumes with $b = 1500 \text{ s/mm}^2$ for Prisma and $b = 1000 \text{ s/mm}^2$ for Skyra platforms to minimize the bias from differences in b -values.⁴¹ The diffusion images were corrected for motion artifacts and susceptibility-induced and eddy current distortions using the HCP pipeline.⁴² We then calculated the diffusion parameters (fractional anisotropy [FA], mean diffusivity [MD], axial diffusivity [AD], and radial diffusivity [RD]) using the FSL DTIFIT tool (FSL version 6.0.4).^{43,44} Next, we registered each FA map onto the JHU WM FA template⁴⁵ using Advanced Neuroimaging Tools⁴⁶ and back projected the JHU WM FA atlas⁴⁵ onto the participant's image to generate 25 regions of interest (ROI) in native space. The detailed methodology and the 25 ROIs were described previously.⁴⁷ Because we had identified a systematic bias in the diffusivities obtained on Skyra relative to those obtained with the Prisma acquisition

parameters, the Skyra diffusivities were multiplied by previously determined scaling factors⁹ to account for the systematic differences due to b -values and voxel size.

MRS Quantification

Preprocessed and averaged spectra were quantified using LCModel⁴⁸ (version 6.3.0G) with a simulated basis set.²⁷ Metabolite concentration estimates were corrected for water T_2 relaxation time, tissue water content, and cerebrospinal fluid contribution.¹⁴ For each VOI, metabolites with mean CRLB $\leq 20\%$ for the entire cohort were included in the statistical analyses. The mean CRLBs were computed considering all the concentrations with the exception for those with fitting failures (CRLB = 999%).

Statistical Analysis

We first analyzed regions and measures known to be affected in SCA1 and SCA3 (*hypothesis-driven approach*), chosen based on previous MRI and postmortem studies (Table S1). Next, we completed an *exploratory analysis* to capture other measures sensitive to short-term progression. To account for differences in follow-up durations between participants, change in each MR measure was computed as the difference between visits (visit 2 minus visit 1) divided by the follow-up duration in years. These slopes were compared between control, SCA1, and SCA3 groups using nonparametric Kruskal–Wallis test. For the exploratory approach only, P -values were Holm–Bonferroni adjusted for multiple comparisons within each MR analysis (for 54 volumes in *FastSurfer/FreeSurfer* volumetry, 40 volumes in CERES volumetry, 25 regions in each dMRI measure [FA; mean/radial/axial diffusivities, MD, RD, AD], 9 metabolites in MRS across both VOIs, and 4 measures in spinal morphometry [C1 and C2 cross-sectional area and eccentricity]). The measures that exhibited statistical significance ($P < 0.05$) in group comparisons underwent pairwise Wilcoxon comparisons between the three groups.

Cohen's d was computed for each SCA–control comparison as the difference in mean slopes divided by the pooled standard deviation. Additionally, the standardized response mean (SRM) was computed for each SCA as the mean change divided by the standard deviation of the change. As the change in MR measures of control participants can be different from 0, a high Cohen's d can be observed with a low SRM and vice versa. Pearson's correlations between change in MR measures and clinical and blood biomarker measures (SARA, neurofilament light chain⁴⁹ [NfL] and estimated time from onset at baseline, SARA change, and CAG repeat size) were calculated for the pooled SCA groups and each SCA separately. To account for type I errors

and because the correlations were not adjusted for multiple comparisons, only correlations of the MR measures that exhibited statistically significant change over time are discussed in Results.

Sample sizes were estimated for two-group interventional trials of 6-month duration using MRI and SARA as outcomes (the latter based on existing large cohort data⁵⁰), for treatment effects varying from 0.5 to 1.0 with power set at 0.8 or 0.9 and α at 0.05.

Statistical tests were performed at the conventional 2-tailed type I error of 0.05. Data were analyzed using R version 4.2.0.

Results

Cohort Characteristics, Data Availability, and QC

We enrolled 44 participants for the 6-month follow-up: 35 patients (10 SCA1, median [IQR] age: 47 [37–54] years, 8 women [80%]; 25 SCA3, median [IQR] age: 42 [37–50], 15 women [60%]) and 9 gene-negative controls (median [IQR] age: 47 [34–51] years, 3 women [33%]). Fifteen participants (13 SCA3, 2 SCA1) were at the preataxic stage (44% of mutation carriers, Table 1). One participant phenoconverted during follow-up. Gene-negative controls were age- and sex matched to mutation carriers. SARA score did not change significantly in either SCA group over this time frame.

Because short-term follow-up data were available only from a subset of the baseline READISCA imaging cohort,⁹ we compared the baseline demographics and ataxia severity of the 44 participants who returned for the 6-month follow-up to the 63 remaining participants from the baseline cohort ($n = 107$) to assess if those who did not return were demographically different or more severely affected (Table S2). There were no statistically significant differences between the two groups ruling out selection bias.

Structural and dMRI data were obtained from all participants (Fig. 1). Upon QC, 1 participant with SCA1 was excluded from the deep gray matter and brainstem volumetry analysis, and 1 participant with SCA3 was excluded from the spinal cord analysis due to segmentation errors (Fig. 1). CBWM MRS data were missing from 3 controls and 1 patient with SCA1, and pons MRS data were missing from 3 controls, 1 patient with SCA1, and 1 patient with SCA3, due to incomplete acquisitions or operator errors when manually prescribing VOL. Upon QC, six pons spectra (1 SCA1 individual, 4 SCA3 individuals, and 1 control) were excluded due to poor shim quality at one of the two visits.

Progressive Atrophy in Early SCA1 and SCA3

Change in total and right cerebellum volumes measured using CERES was significantly different between

groups (total cerebellum, $P = 0.042$; right cerebellum, $P = 0.029$), with the SCA3 versus control comparison driving the difference (SCA1, $P = 0.315$; SCA3, $P = 0.046$) (Fig. 2, Table S3). The right cerebellum volume had a high effect size ($d = 0.84$) and moderate responsiveness (SRM = -0.53) for SCA3. We did not find significant progressive volume loss in the cerebrum or upper spinal cord (Tables S5, S7). The exploratory analysis did not uncover other structural measures sensitive to short-term progression.

Progressive Microstructural Damage in Early SCA1 and SCA3

Change in microstructural measures obtained from the middle cerebellar peduncle (MCP) (FA: SCA1, $P = 0.002$; SCA3, $P = 0.002$; MD: SCA1, $P = 0.017$; SCA3, $P = 0.074$; RD: SCA1, $P = 0.012$; SCA3, $P = 0.014$) and the right corona radiata (CR) (FA: SCA1, $P = 0.004$; SCA3, $P = 0.034$; MD: SCA1, $P = 0.023$; SCA3, $P = 0.023$; RD: SCA1, $P = 0.004$; SCA3, $P = 0.030$) was larger in both SCA groups than in controls, with a decline in FA and an increase in diffusivities over time (Figs. 2 and 3). The effect sizes for dMRI measures were very large in both groups ($d > 1.2$), with the SCA1 cohort presenting higher responsiveness ($|\text{SRM}| > 0.8$) than the SCA3 group ($|\text{SRM}| \sim 0.6$, Tables S9, S11, S13, and S15). The exploratory analysis revealed progressive WM damage in the right superior longitudinal fasciculus (SLF, decreased FA and increased RD) in both groups (Figs. 2 and 3), with the highest effect sizes ($d \sim 2$), but similar responsiveness to MCP and CR (Tables S9 and S15).

Because the significant changes were found in the right hemisphere for both CR and SLF, we evaluated if these changes were driven by a technical reason, such as higher coil sensitivity on the right side. No right/left asymmetry was detected in images and segmentation results. Importantly, cross-sectional group differences in patients versus controls reported previously⁹ were present in the right and left hemispheres at each time point. In addition, the SLF and CR findings were not different between left- and right-handed patients (Wilcoxon $P > 0.05$), indicating findings were not driven by handedness.

Progressive Neurochemical Abnormalities in Early SCA1 and SCA3

Change in neurochemical levels was not significantly different between groups (Tables S17 and S19).

Clinical Correlations

Measures that exhibited significant longitudinal change did not correlate with clinical outcomes (baseline SARA, SARA change, baseline NfL, estimated time from onset at baseline, CAG repeat size). To allow

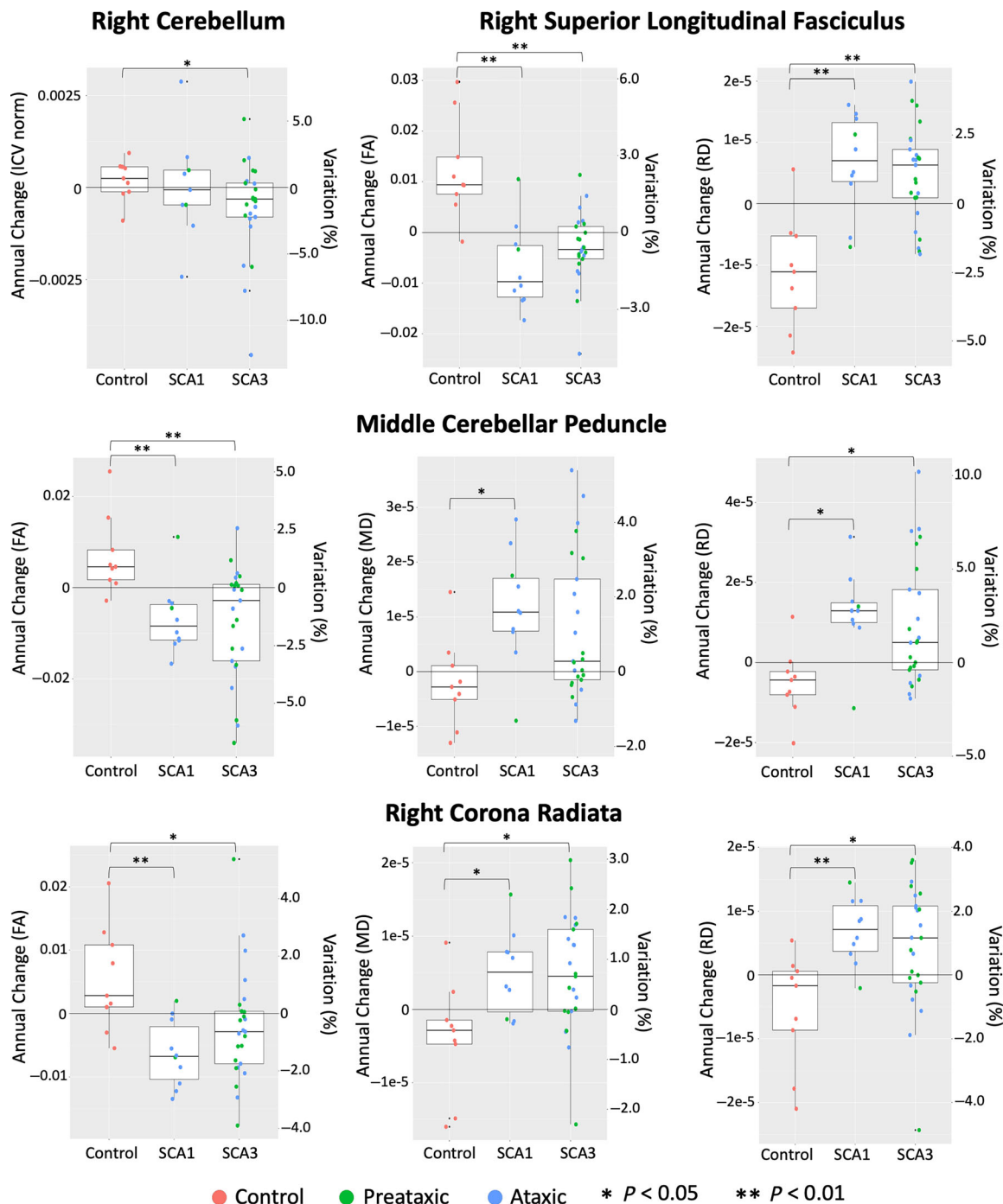


FIG. 2. Magnetic resonance (MR) measures sensitive to 6-month follow-up. Annualized slopes are shown in the units of the MR measure (left y-axis) and % annual change (right y-axis) of the mean cohort value at baseline, with Wilcoxon pairwise P -values ($*P < 0.05$ and $**P < 0.01$).

readers access to the full set of findings, all MR-clinical correlations are presented in Tables S4, S6, S8, S10, S12, S14, S16, S18, and S20.

Sample Size Estimation for Interventional Trials

We estimated sample sizes for clinical trials of 6-month duration with FA of MCP as primary outcome

(Fig. 4). This measure exhibited high responsiveness for both SCAs and is robustly measured across MRI platforms (less sensitive to acquisition parameters than diffusivities). Because no change was detectable in SARA in the small cohort that included preataxic participants, the current data resulted in unrealistic sample sizes with SARA as outcome. To place the MRI-based sample size estimates into context, existing large retrospective

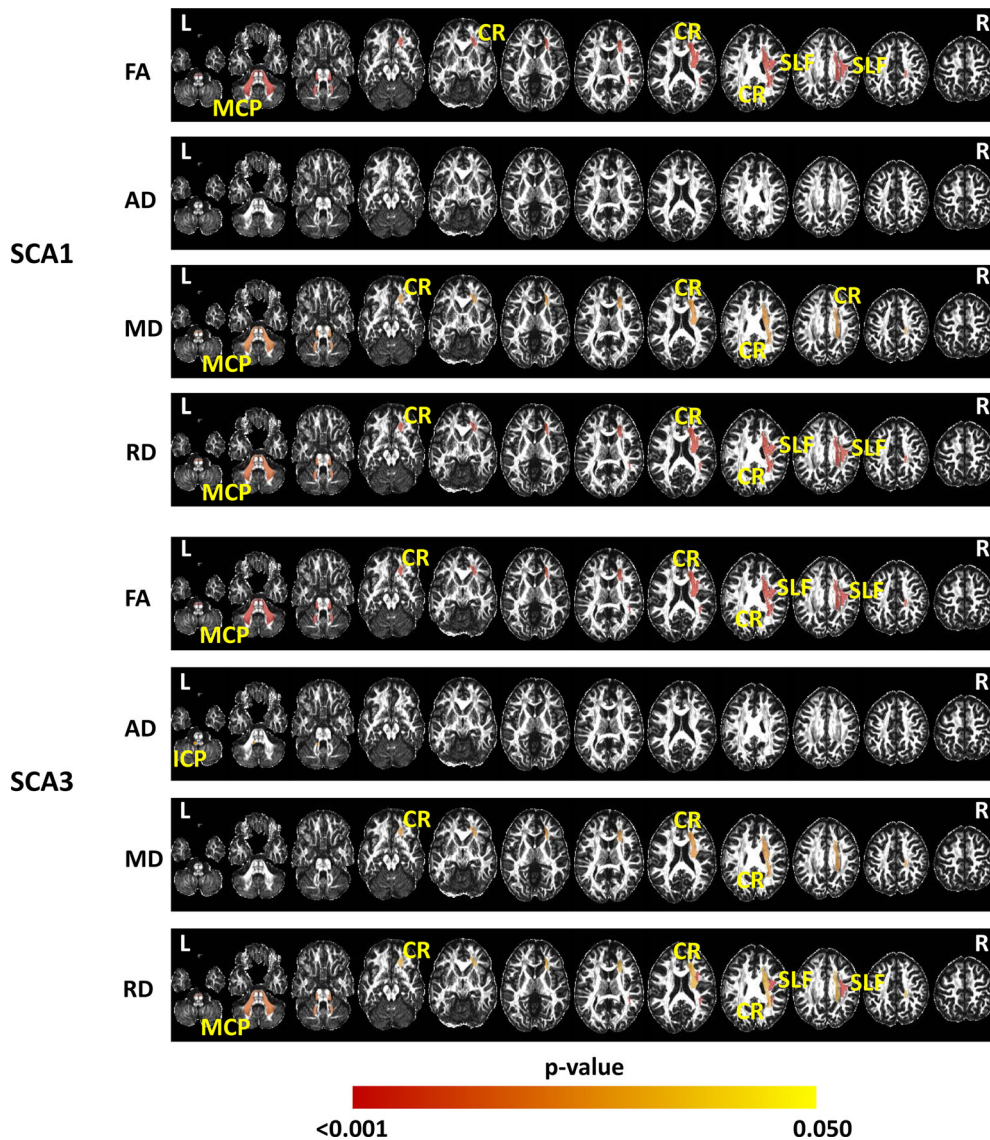


FIG. 3. Progressive microstructural changes. Statistical maps (Wilcoxon P -values for pairwise spinocerebellar ataxia [SCA] vs. control comparisons) are represented on the Johns Hopkins (JHU) atlas fractional anisotropy (FA) map. CR, corona radiata; ICP, inferior cerebellar peduncle; MCP, middle cerebellar peduncle; SLF, superior longitudinal fasciculus.

cohort data⁵⁰ with 186 SCA1 and 272 SCA3 participants (a subset of whom phenoconverted during follow-up) were used to estimate a sample size with SARA as outcome in an early ataxic cohort. These estimates predicted a >5-fold decrease in the sample size needed in trials that would slow progression by 50% to 100% with FA of MCP relative to SARA as outcome measure.

Discussion

We evaluated the sensitivity of advanced multimodal MRI to short-term change in two slowly progressing neurodegenerative diseases in a multisite trial setting. We identified progressive abnormalities in dMRI

measures in major cerebral and cerebellar WM tracts in SCA1 and SCA3 and predicted a substantial sample size reduction with imaging relative to clinical outcomes in interventional trials less than a year, which could significantly reduce costs and allow therapies to reach patients more quickly.

The sensitivity of MRI measures to progressive changes in the brain was previously reported in later-stage SCA cohorts and never with follow-up durations less than a year.¹¹⁻¹⁴ Prior studies showed significant correlations between MRI outcomes and estimated time to/after onset over a 30-plus-year range but did not detect significant progression of these measures over 1 to 2.5 years.^{10,51} Among other slowly progressing neurodegenerative diseases, volumetric measures were sensitive to change over 6 months in Huntington's

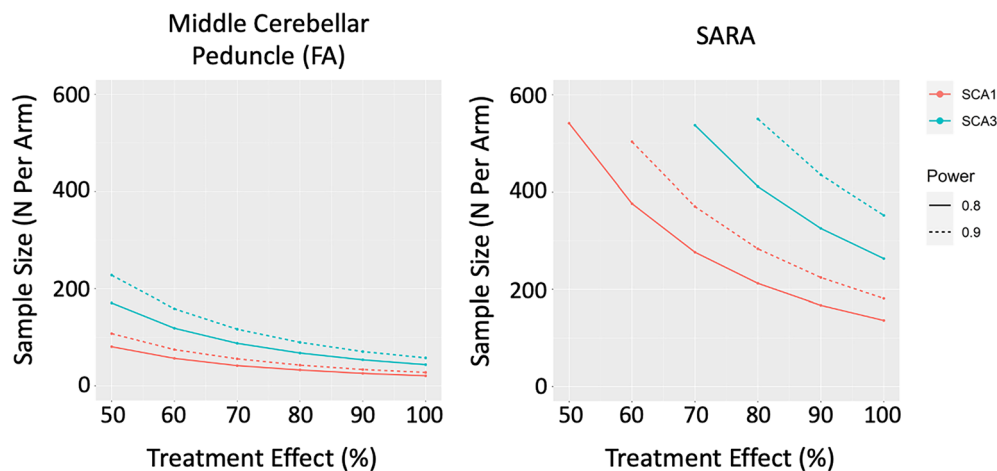


FIG. 4. Sample size estimation for a two-arm interventional trial of 6-month duration to detect a significant difference in progression between a treated and a placebo group of 50% to 100% using fractional anisotropy of middle cerebellar peduncle and Scale for Assessment and Rating of Ataxia (SARA) as primary outcomes.

disease but with smaller effect sizes.⁵² Therefore, such large effect sizes were not observed previously for short follow-up imaging in other slowly progressing neurodegenerative diseases.

Whereas the cerebellum volume was sensitive to change in SCA3 (Fig. 2), dMRI measures had larger effect sizes in both SCAs, consistent with microstructural changes preceding atrophy in early disease stages. Notably, the progressive WM abnormalities without significant cortical atrophy are indicative of axonopathy, as also indicated by cross-sectional data in preataxic and early SCA1 and SCA3.^{9,53} In addition, RD changes were more pronounced than AD, potentially reflecting a progressive demyelinating process⁵⁴ rather than axonal injury and supporting recent findings of oligodendrocyte involvement in SCA1 and SCA3 pathogenesis.⁵⁵

The dMRI measures exhibited higher responsiveness in SCA1 than SCA3, consistent with faster progression in SCA1. Progressive microstructural changes in major cerebral tracts at an early disease stage are somewhat surprising considering the caudal-rostral pattern of degeneration indicated by cross-sectional data in these SCAs.^{9,53} However, the ability to detect subtle changes over time depends on the reproducibility of the measures. CR and SLF provided sensitivity to measure 1% to 2% change (Fig. 2), because they are major tracts with highly reproducible dMRI measurements.⁵⁶ MCP, a smaller tract, but the largest of the three cerebellar peduncles, allowed detection of larger-magnitude dMRI changes. Interestingly, the changes in CR and SLF were consistently in the right brain in both SCAs. We confirmed that this was not a technical artifact (eg, coil sensitivity) nor associated with handedness. A laterality in pathology has not been reported in SCAs; nonetheless, these findings caution against averaging right- and left MR measures to reduce the number of statistical analyses as commonly done.^{51,57} Whether the progressive

pathology is more prominent in the right brain in early SCA1 and SCA3 remains to be confirmed.

Based on the technical sensitivity argument, the progressive dMRI abnormalities may reflect generalized WM damage in these SCAs. Nonetheless, these data suggest early progressive deficits in the functions associated with these tracts. The MCP is the primary cerebellar afferent tract linking cerebral sensorimotor, association, and limbic areas with the cerebellum⁵⁸ and is involved in motor planning and execution.⁵⁹ Therefore, progressive MCP damage likely underlies the development of early ataxic signs and may contribute to the development of the cerebellar cognitive affective syndrome in patients with SCA.⁶⁰ Corticospinal and sensory signs were the earliest clinical findings in the READISCA cohort.⁴⁹ Therefore, the CR findings are likely due to changes in corticospinal fibers passing through this structure. Finally, the SLF is a massive cerebral bundle with substantial functional lateralization, and the right SLF is involved in visuospatial processing and spatial awareness.⁶¹ Visuospatial impairment was noted in later-stage SCA3,⁶² and our finding motivates assessment of visuospatial deficits in early disease.

The sample size for the neurochemical assessments was smaller than the structural and dMRI assessments (Fig. 1), with only five control datasets from the pons. Therefore, the study was underpowered to detect a group difference in the slope of pontine tNAA/Ins, a neuroglial marker that was shown to be sensitive to change over longer follow-up in SCA1.¹⁴ However, its large effect sizes (1.4) and responsiveness ($|\text{SRM}| \geq 0.8$) indicate that faster tNAA/Ins decline than controls will likely be detectable in early SCA1 and SCA3 with appropriate sample sizes.

The primary limitation of this study is the small sample size, particularly for the SCA1 and control groups, and is reflective of challenges with sufficiently powered trials in these rare diseases. Thus, the necessary sample

sizes in the hundreds per arm when utilizing clinical outcomes^{2,63} are prohibitive in SCAs. This was the primary motivation to utilize an advanced MRI protocol with high technical reproducibility that nonetheless is implementable at academic sites, where trials of disease-modifying therapeutics will occur. The small sample size may also have resulted in an overestimation of effect sizes and thereby underestimation of sample sizes using imaging outcomes; however, even a twofold reduction in necessary sample sizes would result in substantial savings and facilitate well-powered trials. Also note that the sample size achieved here was comparable to targeted enrollment in gene-silencing trials recently initiated by industry (<https://clinicaltrials.gov/study/NCT05822908>, <https://clinicaltrials.gov/study/NCT05160558>). A second limitation was that clinical data were limited to SARA. Frequent assessment of pyramidal signs and visuospatial processing at early disease stages is warranted in future studies.

To summarize, select dMRI measures emerge as candidates for tracking the slowing, and perhaps reversal, of SCA1 and SCA3 pathology in early stages in therapeutic trials of ~6-month duration, which is not feasible with clinical outcome measures given the large sample sizes required (Fig. 4). Other MR measures (pontine tCr in SCA1 and RD of inferior cerebellar peduncle in SCA3) were the most sensitive to detect cross-sectional group differences between preataxic gene carriers and controls⁹; however, their poorer test-retest reproducibility⁵⁶ prevents detection of (smaller)

short-term longitudinal change with the current sample sizes. The sample size estimates with dMRI outcomes are still large, that is, 100 to 200 patients needed per arm to detect a 50% reduction in the slope of MCP FA. Longer follow-up durations, for example, 9 months, will further reduce the necessary sample sizes and allow therapeutic trials with MRI outcomes responsive to change in less than a year. ■

Acknowledgments: The READISCA investigators would like to thank all participants for their enduring willingness and interest in this research. We extend our gratitude to Dr. Dinesh Deelchand for assistance with MR protocol development; Brian Hanna for developing the defacing/identification Docker pipeline; Diane Hutter, Ann Fishman, Jason Macmore, Brigitte Jacoby, Samantha Pierce, Jessica Magenheimer, Anke Ruehling, and Hortense Hurmic for study coordination; and Chantel Potvin and Erika Espinoza for project management.

Data Availability Statement

Subject-level clinical and imaging data from READISCA will be available from the National Institute of Mental Health Data Archive (<https://nda.nih.gov/>, Collection C3155).

Appendix A

READISCA Consortium Collaborators

READISCA Consortium Collaborators	Affiliations
Liana Rosenthal, MD, PhD	Johns Hopkins University, Baltimore, MD, USA
Matthew Burns, MD, PhD	University of Florida, Gainesville, FL, USA
Marcus Grobe-Einsler, MD; Demet Oender, MD; Berkan Koyak, MD; Okka Kimmich, MD; Nina Roy, PhD	German Center for Neurodegenerative Diseases (DZNE), Bonn, Germany
Giulia Coarelli, MD, PhD; Claire Ewencyk, MD, PhD; Anna Heinzmann, MD; Pauline Lallemand, MD; Hortense Hurmic, BS	Sorbonne Université, Paris Brain Institute (ICM), Assistance Publique des Hôpitaux de Paris (APHP), France
George Wilmot, MD, PhD; Laura Scorr, MD	Emory University, Atlanta, GA, USA
Puneet Opal, MD, PhD	Northwestern University, Evanston, IL, USA
Sharon Sha, MD; Veronica Santini, MD; Jacinda Sampson, MD	Stanford University, Stanford, CA, USA
Susan Perlman, MD	University of California, Los Angeles, CA, USA
Michael Geschwind, MD, PhD; Alexandra Nelson, MD, PhD; Cameron Dietiker, MD	University of California, San Francisco, CA, USA
Christopher Gomez, MD, PhD	University of Chicago, Chicago, IL, USA
Vikram Shakkottai, MD, PhD	University of Texas Southwestern, Dallas, TX, USA
Sheng-Han Kuo, MD	Columbia University, New York, NY, USA

(Continues)

Appendix Continued

READISCA Consortium Collaborators	Affiliations
Trevor Hawkins, MD	University of Colorado, Boulder, CO, USA
Peter Morrison, DO	University of Rochester, Rochester, NY, USA
Stefan M. Pulst, MD; Karla P. Figueroa, MS	University of Utah, Salt Lake City, UT, USA
Anne-Laure Fauret-Amsellem, MD	Unité de Neurogénétique Moléculaire et Cellulaire, AP-HP, Hôpital Pitié-Salpêtrière, Paris, France
Sylvie Forlani, PhD	Sorbonne Université, Paris Brain Institute–ICM, Inserm, CNRS, AP-HP, Paris, France
Olaf Riess, MD	Institute for Medical Genetics and Applied Genomics, University of Tuebingen, Tuebingen, Germany

References

- Rüb U, Schöls L, Paulson H, et al. Clinical features, neurogenetics and neuropathology of the polyglutamine spinocerebellar ataxias type 1, 2, 3, 6 and 7. *Prog Neurobiol* 2013;104:38–66.
- Ashizawa T, Öz G, Paulson HL. Spinocerebellar ataxias: prospects and challenges for therapy development. *Nat Rev Neurol* 2018;14(10):590–605.
- Rubinsztein DC, Orr HT. Diminishing return for mechanistic therapeutics with neurodegenerative disease duration?: there may be a point in the course of a neurodegenerative condition where therapeutics targeting disease-causing mechanisms are futile. *Bioessays* 2016;38(10):977–980.
- Schmitz-Hübsch T, du Montcel ST, Baliko L, et al. Scale for the assessment and rating of ataxia: development of a new clinical scale. *Neurology* 2006;66(11):1717–1720.
- Jacobi H, du Montcel ST, Romanzetti S, et al. Conversion of individuals at risk for spinocerebellar ataxia types 1, 2, 3, and 6 to manifest ataxia (RISCA): a longitudinal cohort study. *Lancet Neurol* 2020;19(9):738–747.
- Mullard A. NfL makes regulatory debut as neurodegenerative disease biomarker. *Nat Rev Drug Discov* 2023;22(6):431–434.
- Pandolfo M, Reetz K, Darling A, et al. Efficacy and safety of Leriglitazone in patients with Friedreich ataxia: a phase 2 double-blind, randomized controlled trial (FRAMES). *Neurol Genet* 2022;8(6):e200034.
- Budd Haerberlein S, Aisen PS, Barkhof F, et al. Two randomized phase 3 studies of aducanumab in early Alzheimer's disease. *J Prev Alzheimers Dis* 2022;9(2):197–210.
- Chandrasekaran J, Petit E, Park YW, et al. Clinically meaningful magnetic resonance endpoints sensitive to Preataxic spinocerebellar ataxia types 1 and 3. *Ann Neurol* 2023;93(4):686–701.
- de Oliveira CM, Leotti VB, Polita S, et al. The longitudinal progression of MRI changes in pre-ataxic carriers of SCA3/MJD. *J Neurol* 2023;270(9):4276–4287.
- Reetz K, Costa AS, Mirzazade S, et al. Genotype-specific patterns of atrophy progression are more sensitive than clinical decline in SCA1, SCA3 and SCA6. *Brain* 2013;136(Pt 3):905–917.
- Adanyeguh IM, Perlberg V, Henry PG, et al. Autosomal dominant cerebellar ataxias: imaging biomarkers with high effect sizes. *NeuroImage Clinical* 2018;19:858–867.
- Piccinin CC, Rezende TJR, de Paiva JLR, et al. A 5-year longitudinal clinical and magnetic resonance imaging study in spinocerebellar ataxia type 3. *Mov Disord* 2020;35(9):1679–1684.
- Deelchand DK, Joers JM, Ravishankar A, et al. Sensitivity of volumetric magnetic resonance imaging and magnetic resonance spectroscopy to progression of spinocerebellar ataxia type 1. *Mov Disord Clin Pract* 2019;6(7):549–558.
- Tezenas du Montcel S, Durr A, Rakowicz M, et al. Prediction of the age at onset in spinocerebellar ataxia type 1, 2, 3 and 6. *J Med Genet* 2014;51(7):479–486.
- Peng L, Chen Z, Long Z, et al. New model for estimation of the age at onset in spinocerebellar ataxia type 3. *Neurology* 2021;96(23):e2885–e2895.
- Van Essen DC, Smith SM, Barch DM, et al. The WU-Minn human connectome project: an overview. *Neuroimage* 2013;80:62–79.
- Deelchand DK, Berrington A, Noeske R, et al. Across-vendor standardization of semi-LASER for single-voxel MRS at 3T. *NMR Biomed* 2021;34(5):e4218.
- Deelchand DK, Henry PG, Joers JM, et al. Plug-and-play advanced magnetic resonance spectroscopy. *Magn Reson Med* 2022;87(6):2613–2620.
- Park YW, Deelchand DK, Joers JM, et al. AutoVOI: real-time automatic prescription of volume-of-interest for single voxel spectroscopy. *Magn Reson Med* 2018;80(5):1787–1798.
- Archie KA, Marcus DS. DicomBrowser: software for viewing and modifying DICOM metadata. *J Digit Imaging* 2012;25(5):635–645.
- Milchenko M, Marcus D. Obscuring surface anatomy in volumetric imaging data. *Neuroinformatics* 2013;11(1):65–75.
- Backhausen LL, Herting MM, Buse J, Roessner V, Smolka MN, Vetter NC. Quality control of structural MRI images applied using FreeSurfer-A hands-on workflow to rate motion artifacts. *Front Neurosci* 2016;10:558.
- Bastiani M, Cottaar M, Fitzgibbon SP, et al. Automated quality control for within and between studies diffusion MRI data using a non-parametric framework for movement and distortion correction. *Neuroimage* 2019;184:801–812.
- Andersson JLR, Sotiropoulos SN. An integrated approach to correction for off-resonance effects and subject movement in diffusion MR imaging. *Neuroimage* 2016;125:1063–1078.
- Andersson JLR, Graham MS, Drobnjak I, Zhang H, Filippini N, Bastiani M. Towards a comprehensive framework for movement and distortion correction of diffusion MR images: within volume movement. *Neuroimage* 2017;152:450–466.
- Deelchand DK, Adanyeguh IM, Emir UE, et al. Two-site reproducibility of cerebellar and brainstem neurochemical profiles with short-echo, single-voxel MRS at 3T. *Magn Reson Med* 2015;73(5):1718–1725.
- Henschel L, Conjeti S, Estrada S, Diers K, Fischl B, Reuter M. FastSurfer - a fast and accurate deep learning based neuroimaging pipeline. *Neuroimage* 2020;219:117012.
- Fischl B. FreeSurfer. *Neuroimage* 2012;62(2):774–781.
- Henschel L, Kugler D, Reuter M. FastSurferVINN: building resolution-independence into deep learning segmentation methods-a solution for HighRes brain MRI. *Neuroimage* 2022;251:118933.

31. Reuter M, Fischl B. Avoiding asymmetry-induced bias in longitudinal image processing. *Neuroimage* 2011;57(1):19–21.
32. Reuter M, Rosas HD, Fischl B. Highly accurate inverse consistent registration: a robust approach. *Neuroimage* 2010;53(4):1181–1196.
33. Reuter M, Schmansky NJ, Rosas HD, Fischl B. Within-subject template estimation for unbiased longitudinal image analysis. *Neuroimage* 2012;61(4):1402–1418.
34. Iglesias JE, Van Leemput K, Augustinack J, et al. Bayesian longitudinal segmentation of hippocampal substructures in brain MRI using subject-specific atlases. *Neuroimage* 2016;141:542–555.
35. Iglesias JE, Van Leemput K, Bhatt P, et al. Bayesian segmentation of brainstem structures in MRI. *Neuroimage* 2015;113:184–195.
36. Romero JE, Coupe P, Giraud R, et al. CERES: a new cerebellum lobule segmentation method. *Neuroimage* 2017;147:916–924.
37. Cabeza-Ruiz R, Velazquez-Perez L, Linares-Barranco A, Perez-Rodriguez R. Convolutional neural networks for segmenting cerebellar fissures from magnetic resonance imaging. *Sensors* 2022;22(4):1345.
38. Soros P, Wolk L, Bantel C, Brauer A, Klawonn F, Witt K. Replicability, repeatability, and Long-term reproducibility of cerebellar morphometry. *Cerebellum* 2021;20(3):439–453.
39. Rezende TJR, Adanyeguh IM, Arrigoni F, et al. Progressive spinal cord degeneration in Friedreich's ataxia: results from ENIGMA-ataxia. *Mov Disord* 2023;38(1):45–56.
40. De Leener B, Levy S, Dupont SM, et al. SCT: spinal cord toolbox, an open-source software for processing spinal cord MRI data. *Neuroimage* 2017;145:24–43.
41. Papinutto ND, Maule F, Jovicich J. Reproducibility and biases in high field brain diffusion MRI: an evaluation of acquisition and analysis variables. *Magn Reson Imaging* 2013;31(6):827–839.
42. Glasser MF, Sotiropoulos SN, Wilson JA, et al. The minimal preprocessing pipelines for the human connectome project. *Neuroimage* 2013;80:105–124.
43. Behrens TE, Woolrich MW, Jenkinson M, et al. Characterization and propagation of uncertainty in diffusion-weighted MR imaging. *Magn Reson Med* 2003;50(5):1077–1088.
44. Jbabdi S, Sotiropoulos SN, Savio AM, Grana M, Behrens TE. Model-based analysis of multishell diffusion MR data for tractography: how to get over fitting problems. *Magn Reson Med* 2012;68(6):1846–1855.
45. Hua K, Zhang J, Wakana S, et al. Tract probability maps in stereotaxic spaces: analyses of white matter anatomy and tract-specific quantification. *Neuroimage* 2008;39(1):336–347.
46. Avants BB, Tustison NJ, Song G, Cook PA, Klein A, Gee JC. A reproducible evaluation of ANTs similarity metric performance in brain image registration. *Neuroimage* 2011;54(3):2033–2044.
47. Park YW, Joers JM, Guo B, et al. Assessment of cerebral and cerebellar white matter microstructure in spinocerebellar ataxias 1, 2, 3, and 6 using diffusion MRI. *Front Neurol* 2020;11:411.
48. Provencher SW. Estimation of metabolite concentrations from localized in vivo proton NMR spectra. *Magn Reson Med* 1993;30(6):672–679.
49. Tezenas du Montcel S, Petit E, Olubajo T, et al. Baseline clinical and blood biomarkers in patients with Preataxic and early-stage disease spinocerebellar ataxia 1 and 3. *Neurology* 2023;100(17):e1836–e1848.
50. Moulaire P, Poulet PE, Petit E, et al. Temporal dynamics of the scale for the assessment and rating of ataxia in spinocerebellar ataxias. *Mov Disord* 2023;38(1):35–44.
51. Nigri A, Sarro L, Mongelli A, et al. Spinocerebellar ataxia type 1: one-year longitudinal study to identify clinical and MRI measures of disease progression in patients and Presymptomatic carriers. *Cerebellum* 2022;21(1):133–144.
52. Hobbs NZ, Farmer RE, Rees EM, et al. Short-interval observational data to inform clinical trial design in Huntington's disease. *J Neuro Neurosurg Psychiatry* 2015;86(12):1291–1298.
53. Rezende TJR, de Paiva JLR, Martinez ARM, et al. Structural signature of SCA3: from presymptomatic to late disease stages. *Ann Neurol* 2018;84(3):401–408.
54. Klawiter EC, Schmidt RE, Trinkaus K, et al. Radial diffusivity predicts demyelination in ex vivo multiple sclerosis spinal cords. *Neuroimage* 2011;55(4):1454–1460.
55. Putka AF, Mato JP, McLoughlin HS. Myelinating glia: potential therapeutic targets in polyglutamine spinocerebellar ataxias. *Cells* 2023;12(4):601.
56. Rezende TJR, Campos BM, Hsu J, et al. Test-retest reproducibility of a multi-atlas automated segmentation tool on multimodality brain MRI. *Brain Behav* 2019;9(10):e01363.
57. Faber J, Schaprian T, Berkan K, et al. Regional brain and spinal cord volume loss in spinocerebellar ataxia type 3. *Mov Disord* 2021;36(10):2273–2281.
58. Schmahmann JD. From movement to thought: anatomic substrates of the cerebellar contribution to cognitive processing. *Hum Brain Mapp* 1996;4(3):174–198.
59. Morales H, Tomsick T. Middle cerebellar peduncles: magnetic resonance imaging and pathophysiologic correlate. *World J Radiol* 2015;7(12):438–447.
60. Selvadurai LP, Perlman SL, Ashizawa T, et al. The cerebellar cognitive affective/Schmahmann syndrome scale in spinocerebellar ataxias. *Cerebellum* 2024. <https://doi.org/10.1007/s12311-023-01651-0>
61. Janelle F, Iorio-Morin C, D'Amour S, Fortin D. Superior longitudinal fasciculus: a review of the anatomical descriptions with functional correlates. *Front Neurol* 2022;13:794618.
62. Kawai Y, Takeda A, Abe Y, Washimi Y, Tanaka F, Sobue G. Cognitive impairments in Machado-Joseph disease. *Arch Neurol* 2004;61(11):1757–1760.
63. Jacobi H, du Montcel ST, Bauer P, et al. Long-term disease progression in spinocerebellar ataxia types 1, 2, 3, and 6: a longitudinal cohort study. *Lancet Neurol* 2015;14(11):1101–1108.

Supporting Data

Additional Supporting Information may be found in the online version of this article at the publisher's web-site.